this effect, indicating that the reduction in T_2 is due to low-frequency noise, which we attribute to magnetic domain noise of the tip material. We expect that this effect can be mitigated using alternative tip materials such as rare earth ferromagnets (*27*). The coupling strength can be further improved by using customized nanoresonators with a larger zero-point motion. Using state-of-the-art nanofabrication techniques, resonators with $Q > 10^6$, $\omega_r/2\pi \sim 1$ MHz (*28*), $G_m \sim 10^5$ T/m, and a coupling strength of $\lambda/2\pi \sim 10$ kHz can be fabricated (*4*), which, together with extended coherence times in isotopically purified diamond of $T_2 > 2$ ms (*29*) and faster pulse sequences with $N \sim 136$ pulses (*23*), yield a projected sensitivity of $\eta < 1$ phonon/$\sqrt{\text{Hz}}$. Combined with recently demonstrated single-shot spin readout (*30*), this raises the intriguing prospect of using a single NV center to sense mechanical motion at the scale of zero-point fluctuations in a single shot.

To assess the feasibility of sensing zero-point motion (Fig. 4A), we assume that the resonator is actively cooled near its motional ground state, using either the spin (*4*) or an additional system such as an optical or microwave cavity (*12*, *13*). Such cooling schemes are always accompanied by a decreased effective mechanical quality factor, $Q_{\text{eff}} = Q/\overline{n}_{\text{env}}$, where $\overline{n}_{\text{env}}$ is the phonon occupation number at the temperature of the surrounding environment. Inserting $\overline{n}_{\text{th}} = 0$ and $W = 2Q_{\text{eff}}/N$ into Eq. 1, a near maximal signal $S \sim 1/2$ is obtained, provided that $C = \lambda^2 Q_{\text{eff}} \tilde{T}_2/\omega_r > 1$, where $\tilde{T}_2 = T_2 N^{2/3}$ is the extended spin-coherence time due to dynamical decoupling (*23*). This is verified in Fig. 4B, which demonstrates that for a wide range of realistic parameters with $C > 1$, the zero-point motion of the resonator results in $S \sim 1/2$. The parameter C is a fundamental quantity in the physics of spin-phonon interactions. In direct analogy to the so-called cooperativity in cQED, $C > 1$ marks the onset of coherent quantum effects in a coupled spin-phonon system. Taking the optimized but realistic values $\lambda/2\pi = 10$ kHz, $T_2 = 1$ ms, $Q = 10^6$, $\omega_r/2\pi = 1$ MHz, and $N = 160$ pulses, we find that $C \sim 35$ can be reached at an environmental temperature of $T = 4$ K. Besides detection of zero-point motion, entering this regime could also enable coherent, long-range interactions between individual spins mediated by a mechanical resonator (*17*), which are of great interest for developing scalable, spin-based quantum information systems. Furthermore, by operating at lower environmental temperatures of $T \sim 100$ mK, it becomes possible to use the spin to cool the resonator down to its ground state (*4*) and to engineer quantum superpositions of mechanical motion, which could be read out using a coherent detection scheme like the one we present in this work.

The above considerations indicate that our approach provides an experimentally feasible route toward reaching strong coupling between single phonons and spins. Potential applications ranging from the creation and detection of quantum states of mechanical motion and the realization of quantum spin transducers to novel approaches for nanoscale sensing and readout (*19*, *20*) can be foreseen.

References and Notes

1. M. Scully, M. Zubairy, *Quantum Optics* (Cambridge Univ. Press, Cambridge, 1997).
2. S. Haroche, J. Raimond, *Exploring the Quantum: Atoms, Cavities, and Photons* (Oxford Univ. Press, New York, 2006).
3. R. J. Schoelkopf, S. M. Girvin, *Nature* **451**, 664 (2008).
4. P. Rabl *et al.*, *Phys. Rev. B* **79**, 041302 (2009).
5. P. Treutlein, D. Hunger, S. Camerer, T. W. Hänsch, J. Reichel, *Phys. Rev. Lett.* **99**, 140403 (2007).
6. F. Xue, L. Zhong, Y. Li, C. P. Sun, *Phys. Rev. B* **75**, 033407 (2007).
7. I. Bargatin, M. L. Roukes, *Phys. Rev. Lett.* **91**, 138302 (2003).
8. T. J. Kippenberg, K. J. Vahala, *Science* **321**, 1172 (2008).
9. G. A. Steele *et al.*, *Science* **325**, 1103 (2009).
10. D. Hunger *et al.*, *Phys. Rev. Lett.* **104**, 143002 (2010).
11. A. D. O'Connell *et al.*, *Nature* **464**, 697 (2010).
12. J. D. Teufel *et al.*, *Nature* **475**, 359 (2011).
13. J. Chan *et al.*, *Nature* **478**, 89 (2011).
14. M. D. LaHaye, J. Suh, P. M. Echternach, K. C. Schwab, M. L. Roukes, *Nature* **459**, 960 (2009).
15. O. Arcizet *et al.*, *Nat. Phys.* **7**, 879 (2011).
16. D. Rugar, R. Budakian, H. J. Mamin, B. W. Chui, *Nature* **430**, 329 (2004).
17. P. Rabl *et al.*, *Nat. Phys.* **6**, 602 (2010).
18. G. Balasubramanian *et al.*, *Nature* **455**, 648 (2008).
19. M. Grinolds *et al.*, *Nat. Phys.* **7**, 687 (2011).
20. C. Degen, *Appl. Phys. Lett.* **92**, 243111 (2008).
21. S. Kotler, N. Akerman, Y. Glickman, A. Keselman, R. Ozeri, *Nature* **473**, 61 (2011).
22. J. R. Maze *et al.*, *Nature* **455**, 644 (2008).
23. G. de Lange, Z. H. Wang, D. Ristè, V. V. Dobrovitski, R. Hanson, *Science* **330**, 60 (2010).
24. Materials and methods are available as supporting material on *Science* Online.
25. J. Taylor *et al.*, *Nat. Phys.* **4**, 810 (2008).
26. L. Childress *et al.*, *Science* **314**, 281 (2006).
27. B. C. Stipe, H. J. Mamin, T. D. Stowe, T. W. Kenny, D. Rugar, *Phys. Rev. Lett.* **86**, 2874 (2001).
28. S. S. Verbridge, H. G. Craighead, J. M. Parpia, *Appl. Phys. Lett.* **92**, 013112 (2008).
29. G. Balasubramanian *et al.*, *Nat. Mater.* **8**, 383 (2009).
30. L. Robledo *et al.*, *Nature* **477**, 574 (2011).

Acknowledgments: We thank T. Baart, M. Grinolds, P. Maletinsky, S. Hong, and A. Yacoby for stimulating discussions and R. Ilic, F. Koppens, and A. Zibrov for early contributions to the experiment. This work was supported in part by the NSF, the Center for Ultracold Atoms, the Air Force Office of Scientific Research Multidisciplinary University Research Initiative, the Defense Advanced Research Projects Agency Quantum-Assisted Sensing and Readout, the European Union (EU) Diamond-Based Atomic Nanotechnologies, and the Packard Foundation. S.K. acknowledges support by the U.S. Department of Defense through the National Defense Science and Engineering Graduate Program and the NSF through the Graduate Research Fellowship Program under grant no. DGE-1144152. Q.U. acknowledges support from Deutschen Forschungsgemeinschaft, and P.R. acknowledges support by the EU network Atomic Quantum Technologies Integrating Project and the Austrian Science Fund (FWF) through Sonderforschungsbereich FOQUS and the START grant Y 591-N16.

Supporting Online Material

www.sciencemag.org/cgi/content/full/science.1216821/DC1
Materials and Methods
SOM Text
Figs. S1 to S3
Tables S1 and S2
References

18 November 2011; accepted 8 February 2012
Published online 23 February 2012;
10.1126/science.1216821

Hydrocarbon Separations in a Metal-Organic Framework with Open Iron(II) Coordination Sites

Eric D. Bloch,[1] Wendy L. Queen,[1,2] Rajamani Krishna,[3] Joseph M. Zadrozny,[1] Craig M. Brown,[2,4] Jeffrey R. Long[1,5]*

The energy costs associated with large-scale industrial separation of light hydrocarbons by cryogenic distillation could potentially be lowered through development of selective solid adsorbents that operate at higher temperatures. Here, the metal-organic framework $Fe_2(dobdc)$ ($dobdc^{4-}$: 2,5-dioxido-1,4-benzenedicarboxylate) is demonstrated to exhibit excellent performance characteristics for separation of ethylene/ethane and propylene/propane mixtures at 318 kelvin. Breakthrough data obtained for these mixtures provide experimental validation of simulations, which in turn predict high selectivities and capacities of this material for the fractionation of methane/ethane/ethylene/acetylene mixtures, removal of acetylene impurities from ethylene, and membrane-based olefin/paraffin separations. Neutron powder diffraction data confirm a side-on coordination of acetylene, ethylene, and propylene at the iron(II) centers, while also providing solid-state structural characterization of the much weaker interactions of ethane and propane with the metal.

As a consequence of the similar sizes and volatilities of the molecules, separations of olefin/paraffin mixtures, such as ethylene/ethane and propylene/propane, must currently be performed at low temperatures and high pressures and are among the most energy-intensive separations carried out at large scale in the chemical industry (*1*). Because these gas mixtures are produced by cracking long-chain hydrocarbons at elevated temperatures, a substantial energy penalty arises from cooling the gases to the low temperatures required for distillation. Thus, tremendous energy savings could be realized if materials enabling the efficient separation of olefins and paraffins at higher temperatures (than currently used in distillation) and atmo-

spheric pressure were achieved. Competing approaches toward this end include membrane designs (*2*) and organic solvent-based sorbents (*3*), as well as porous solid adsorbents featuring selective chemical interactions with the carbon-carbon double bond in olefins. In this latter category, metal-organic frameworks (MOFs), which offer high surface areas, adjustable pore dimensions, and chemical tunability, have received considerable attention as adsorbents in gas storage and gas separation applications, with particular emphasis on the dense storage of methane (*4*, *5*) and hydrogen (*6*, *7*) and on the efficient removal of carbon dioxide from flue gas (*8*) and natural gas deposits (*9*, *10*). More recently, the potential utility of these porous structures for the separation of hydrocarbon mixtures has been exposed (*11*–*15*), specifically for the separation of ethylene/ethane and propylene/propane mixtures. Herein, we show that Fe_2(dobdc), a metal-organic framework with exposed iron(II) coordination sites exhibiting high olefin/paraffin selectivities, can be used for the separation of ethylene/ethane and propylene/propane. Furthermore, simulations that are validated by the experimental work presented here allow us to predict that this framework may be further capable of removing acetylene from the ethylene produced by a naphtha cracker and fractionating a methane/ethane/ethylene/acetylene mixture into its pure components. These simulations further predict that Fe_2(dobdc) exhibits higher adsorption selectivities and hydrocarbon separation capacity than a number of recently reported solid adsorbents.

The redox-active metal-organic framework Fe_2(dobdc) (dobdc^{4-} : 2,5-dioxido-1,4-benzenedicarboxylate), also referred to as Fe-MOF-74 or CPO-27-Fe, was selected for testing in separating olefin/paraffin mixtures owing to its previously demonstrated ability to bind O_2 at the iron centers in a side-on manner (*16*). This framework displays a Brunauer-Emmett-Teller surface area of 1350 m^2/g and 11 Å–wide channels lined with square pyramidal Fe^{2+} cations, each with an open coordination site accessible to incoming adsorbate molecules (Fig. 1). With a compact tetra-anionic bridging ligand, the structure features an extremely high surface density of 2.9 Fe^{II} coordination sites available per 100 $Å^2$ on its surface, with spacings of just 6.84(1) and 8.98(2) Å between iron atoms along and around a channel, respectively. Thus, it appears to provide a near-optimal platform for the high-capacity adsorption of small olefins, such as ethylene and propylene. Furthermore, the Mg^{2+} or Co^{2+} analogs of this structure type have recently been shown to display selective adsorption for olefins over paraffins (*17*, *18*). The higher surface area and softer metal character of Fe_2(dobdc) as compared to the recently reported materials should lend both higher selectivity and capacity to the iron(II) framework.

To investigate the ability of Fe_2(dobdc) to adsorb light hydrocarbons, pure component equilibrium adsorption isotherms for methane, ethane, ethylene, acetylene, propane, and propylene were measured at 318, 333, and 353 K. Figure 2 shows the data obtained at 318 K, with the remaining data presented in fig. S1. As evidenced by the initial steep rise in the isotherms, Fe_2(dobdc) displays a strong affinity for the unsaturated hydrocarbons acetylene, ethylene, and propylene. Additionally, the uptake of these gases at 1 bar approaches the stoichiometric quantity expected if one gas molecule is adsorbed per iron(II) center. The propane and ethane adsorption capacities under these conditions, although lower than those of their unsaturated counterparts, are both considerably higher than observed for methane, which has a lower polarizability and a smaller kinetic diameter. Importantly, all of the isotherms are completely reversible and exhibit no hysteresis. Further equilibrium adsorption experiments at 318 K (fig. S2) indicate no loss in olefin uptake capacity over 15 ethylene adsorption/desorption cycles. Additionally, no loss in propylene uptake was observed after 40 adsorption/desorption cycles, as verified by thermogravimetric analysis (fig. S2).

Neutron powder diffraction experiments were carried out to determine the nature of the interactions of these adsorbate molecules within Fe_2(dobdc). In a typical experiment, Fe_2(dobdc) was dosed with deuterated gas at 300 K and cooled to 4 K for data collection. Rietveld refinements were performed against these data to provide the structural models presented in Fig. 1. We recently employed this technique to investigate the coordination of dioxygen to the iron centers of this material (*16*). Analogous to these previous results, only one adsorption site is apparent, corresponding to the open coordination site of the exposed Fe^{2+} cations, upon dosing substoichiometric equivalents of gas per framework iron. The unsaturated hydrocarbons acetylene, ethylene, and propylene indeed display the anticipated side-on binding modes, with Fe-C distances lying in the range 2.42(2) to 2.60(2) Å. These distances are sub-

[1]Department of Chemistry, University of California, Berkeley, CA 94720, USA. [2]Center for Neutron Research, National Institute of Standards and Technology, Gaithersburg, MD 20899, USA. [3]Van't Hoff Institute for Molecular Sciences, University of Amsterdam, Science Park 904, 1098 XH Amsterdam, Netherlands. [4]The Bragg Institute, Australian Nuclear Science and Technology Organisation, PMB1, Menai, NSW, Australia. [5]Materials Sciences Division, Lawrence Berkeley National Laboratory, Berkeley, CA 94720, USA.

*To whom correspondence should be addressed. E-mail: jrlong@berkeley.edu.

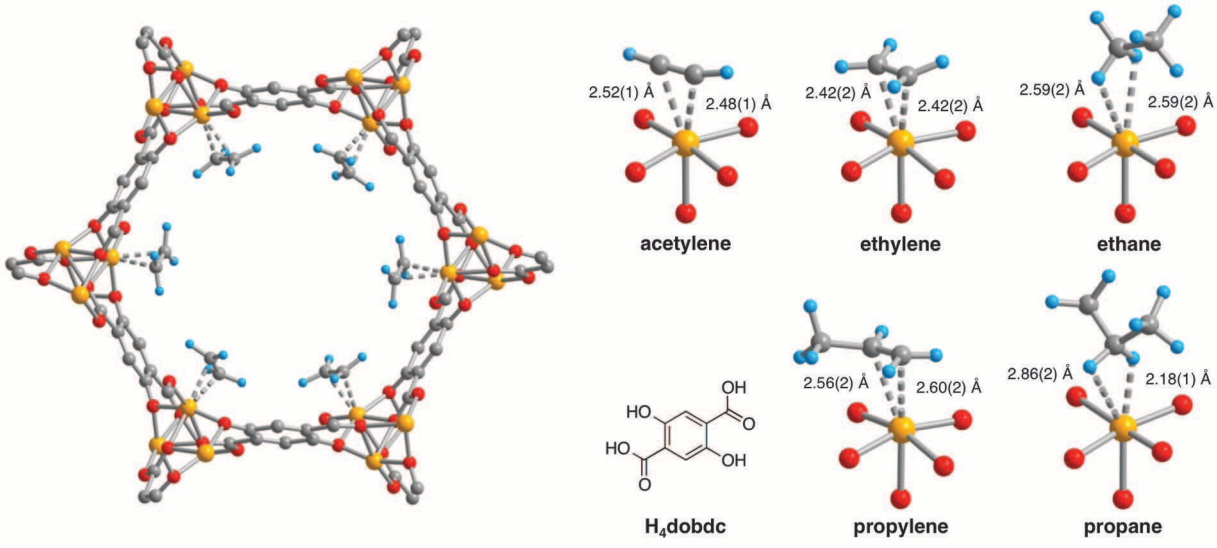

Fig. 1. (**Left**) A portion of the solid-state structure of Fe_2(dobdc)·$2C_2D_4$ as determined by analysis of neutron powder diffraction data; orange, red, gray, and blue spheres represent Fe, O, C, and D atoms, respectively. The view is along the [001] direction and shows an ethylene molecule bound to the open coordination site at each iron(II) center. (**Right**) H_4(dobdc) ligand and the first coordination spheres for the iron centers in the solid-state structures obtained upon dosing Fe_2(dobdc) with acetylene, ethylene, ethane, propylene, and propane. For propane in Fe_2(dobdc), the adsorbed hydrocarbon molecule has orientational disorder with respect to the open metal center. Of several refined models, the single molecule with large displacement parameters is the most reasonable.

stantially longer than the separations of 2.020(5) to 2.078(4) Å observed for the diamagnetic complex $[Fe(C_2H_4)_4]^{2-}$, one of the very few iron(II)-olefin species to be structurally characterized previously (*19*). The difference suggests that the metal centers within Fe_2(dobdc) maintain a high-spin electron configuration when binding these gases, consistent with weaker interactions that can be reversed with little energy penalty. The interactions of both ethane and propane with the metal cations in Fe_2(dobdc) are even weaker, as evidenced by the elongated Fe-C distance of ~3 Å. This is in good agreement with the Mg-C distance reported for methane adsorption in Mg_2(dobdc), a system in which the metal-adsorbate interactions are also a result of ion-induced dipole interactions between coordinatively unsaturated metal cations and a hydrocarbon (*20*).

Variable-temperature magnetic susceptibility measurements were performed to probe the electronic state of the iron centers in Fe_2(dobdc) upon gas binding. As shown in Fig. 3, Fe_2(dobdc) itself displays a $\chi_M T$ value of 6.40 cm^3K/mol at 300 K, which gradually rises as the temperature decreases before turning over and dropping sharply below 28 K. The behavior is consistent with the presence of high-spin (S = 2) iron(II) centers exhibiting weak [J = 4.1(1) cm^{-1}] ferromagnetic coupling along the oxo-bridged chains running parallel to the c axis, together with still weaker antiferromagnetic coupling between chains. Under a pressure of 1 bar of methane, ethane, ethylene, acetylene, propane, or propylene, the high-spin electron configuration of the iron(II) centers is maintained, but the nature of the magnetic exchange along the chains is altered to varying extents. Weakly interacting adsorbates, such as methane, ethane, and propane, slightly diminish the strength of the ferromagnetic exchange, whereas the more strongly interacting propylene, ethylene, and acetylene perturb the electron density at the iron(II) centers sufficiently to reverse the nature of the intrachain coupling from ferromagnetic to antiferromagnetic. Moreover, the J values resulting from the fits to the data provide a qualitative measure of the adsorbate binding energy, suggesting that the strength of the iron(II)-hydrocarbon interactions increase along the series methane < ethane < propane < propylene < acetylene < ethylene.

The strength of hydrocarbon binding within Fe_2(dobdc) was determined quantitatively through analysis of the gas adsorption data. The data for acetylene, ethylene, ethane, propane, and propylene, expressed in terms of absolute loadings, were fitted with the dual-Langmuir-Freundlich isotherm model, whereas methane adsorption data were fitted with a single-site Langmuir model (*21*). Isosteric heats of adsorption were then calculated from the fits to compare the binding enthalpies of these gases under various loadings (fig. S3). Heats of adsorption for acetylene (–47 kJ/mol), ethylene (–45 kJ/mol), and propylene (–44 kJ/mol) show a significant reduction as the loading approaches the value corresponding to one gas molecule per iron(II) center, again consistent with the exposed metal cations presenting the strongest adsorption sites in the material. Propane (–33 kJ/mol), ethane (–25 kJ/mol), and methane (–20 kJ/mol) adsorption enthalpies are all considerably lower in magnitude, with the trend reflecting the decreasing polarizabilities of these molecules from propane to ethane to methane.

Adsorption selectivities were calculated using ideal adsorbed solution theory (IAST) (*22*), using the fitted isotherms of the experimental isotherm data for relevant gas mixtures in Fe_2(dobdc) and a number of other porous materials for which analogous gas uptake properties have been reported (fig. S4). For an equimolar mixture of ethylene and ethane at 318 K, the adsorption selectivities obtained for Fe_2(dobdc) of 13 to 18 are significantly greater than those calculated for either zeolite NaX or the isostructural metal-organic framework Mg_2(dobdc), which display selectivities of 9 to 14 and 4 to 7, respectively (*17*, *23*). The latter result is consistent with the softer character of Fe^{2+} relative to Mg^{2+}, leading to a stronger interaction with the π electron cloud of the olefin. Similarly, in comparing the performance of Fe_2(dobdc) with other porous materials for the separation of a propane/propylene mixture (selectivity = 13 to 15), it is rivaled in selectivity only by zeolite ITQ-12, which displays adsorption selectivity of 15 while the other materials display selectivities from 3 to 9 (*24*). However,

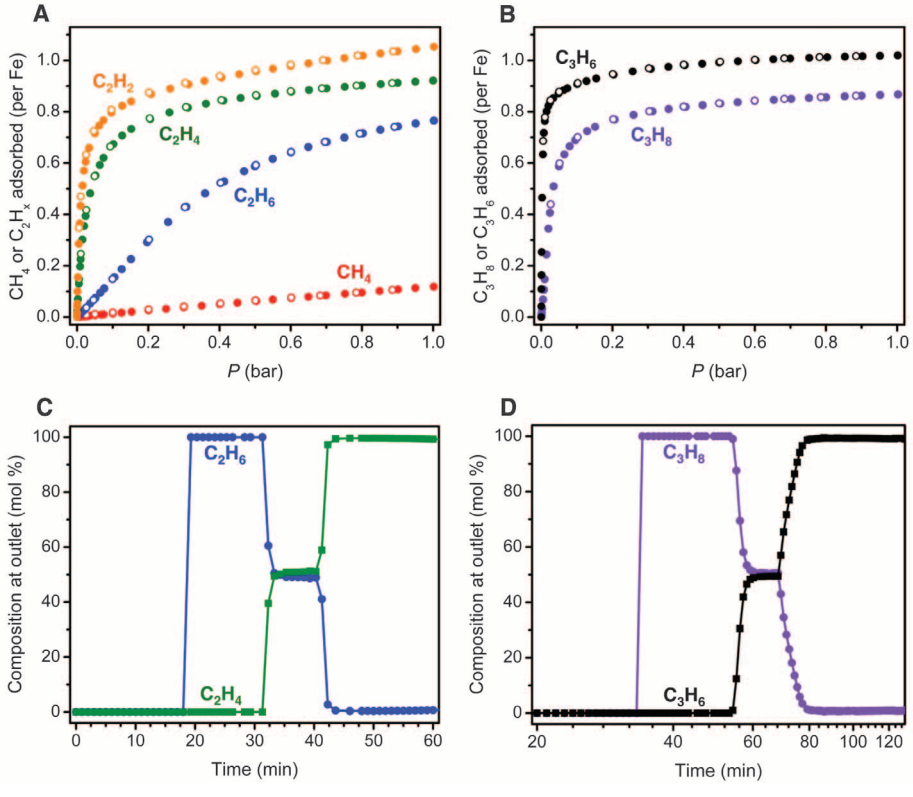

Fig. 2. (**A** and **B**) Gas adsorption isotherms for (A) methane, ethane, ethylene, and acetylene and (B) propane and propylene in Fe_2(dobdc) at 318 K. Filled and open circles represent adsorption and desorption data, respectively. The adsorption capacities at 1 bar correspond to 0.77, 5.00, 6.02, 6.89, 5.67, and 6.66 mmol/g, respectively. (**C** and **D**) Experimental breakthrough curves for the adsorption of equimolar (C) ethane/ethylene and (D) propane/propylene mixtures flowing through a 1.5-mL bed of Fe_2(dobdc) at 318 K with a total gas flow of 2 mL/minute at atmospheric pressure. After breakthrough of the olefin and return to an equimolar mixture composition, a nitrogen purge was applied, leading to desorption of the olefin. In an actual separation scenario, desorption would instead be carried out by applying a vacuum and/or raising the temperature.

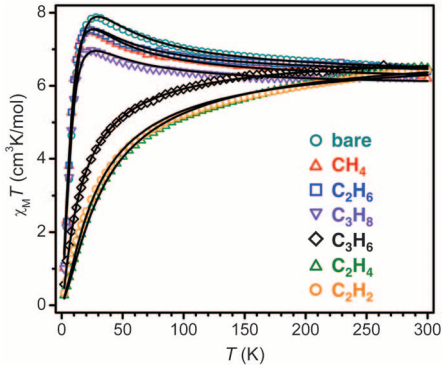

Fig. 3. Variable-temperature magnetic susceptibility data in an applied field of 1 kOe for samples of Fe_2(dobdc) in a vacuum (bare) and under 1 bar of the indicated hydrocarbon. Black lines represent fits to a Hamiltonian derived using the Fisher model for a one-dimensional chain of exchange-coupled S = 2 ions, with an additional term to account for interchain coupling. Full details of the model and fit parameters can be found in table S17 and accompanying text.

the selectivities of ITQ-12 for this mixture were calculated from data collected at 303 K, and it is expected that the selectivity of this material will be lower at higher temperatures. Adsorption selectivities were also calculated using IAST for Fe_2(dobdc) in an equimolar four-component mixture of methane, ethane, ethylene, and acetylene at 318 K, as relating to the purification of natural gas. For an adsorption-based process operating at 1 bar, the calculated acetylene/methane, ethylene/methane, and ethane/methane selectivities are 700, 300, and 20, respectively. These values are much higher than those recently reported (13.8, 11.1, and 16.6, respectively) for a zinc-based metal-organic framework, also based on an analogous calculation procedure (*25*).

To evaluate the performance of Fe_2(dobdc) in an actual adsorption-based separation process, breakthrough experiments were performed in which an equimolar ethylene/ethane or propylene/propane mixture was flowed over a packed bed of the solid with a total flow of 2 mL per minute at 318 K (Fig. 2). In a typical experiment, the gas mixture was flowed through 300 to 400 mg of metal-organic framework crystallites packed into a 1.5-mL glass column, and the outlet gas stream was monitored by a gas chromatograph equipped with a flame ionization detector. As expected from the calculated selectivities, in each case, the alkane was first to elute through the bed, whereas the solid adsorbent retained the olefin. For the C_3 hydrocarbons, the outlet gas contained undetectable levels of propylene, resulting in a propane feed that appeared to be 100% pure, within the detection limit of the instrument [~100 parts per million (ppm)]. Upon saturation of the metal centers within the adsorbent, propylene "broke through," and the outlet gas stream then quickly reached equimolar concentrations. By stopping the gas feed and flowing a purge of nitrogen through the bed, the small amount of weakly bound propane remaining in the pores of the framework could be quickly removed, and the iron-bound propylene then desorbed more slowly. Greater than 99% pure propylene was realized during the desorption step of the breakthrough experiment. In a similar manner, breakthrough experiments showed that Fe_2(dobdc) can separate an equimolar mixture of ethylene and ethane into the pure component gases of 99% to 99.5% purity. Differential scanning calorimetry (DSC) experiments (fig. S5) indicate that energies of 0.84 MJ/kg and 1.3 MJ/kg are needed to release propylene and ethylene, respectively, and regenerate the material for subsequent separation steps.

Although breakthrough experiments are quite valuable for evaluating the gas separation capabilities of a material, in practice they can be difficult and time consuming. In order to compare Fe_2(dobdc) with other reported adsorbents for ethylene/ethane and propylene/propane separations, we sought to demonstrate that the breakthrough characteristics could instead be simulated with reasonable accuracy. Assuming that (i) intracrystalline diffusion is negligible through an isothermal adsorption bed in thermodynamic equilibrium, (ii) plug flow proceeds through the bed, and (iii) the binary mixture adsorption equilibrium in the packed bed of crystallites can be calculated using IAST, we were able to solve a set of partial differential equations and calculate breakthrough curves for both ethylene/ethane and propylene/propane mixtures. The resulting transient gas composition profiles (figs. S6 and S7) are in excellent agreement with the experimental results shown in Fig. 1.

Given this validation, we employed analogous simulations to make quantitative comparisons with other materials. From the simulated breakthrough curves, the time interval during which the exit gas compositions have a purity of 99% propane can be determined, together with the amount of 99% pure propane produced in this time interval. The production capacities, expressed as the amount of propane produced per liter of adsorbent, are shown in fig. S8 over a range of pressures for the zeolites ITQ-12 at 303 K and NaX at 318 K, and for the metal-organic frameworks $Cu_3(btc)_2$ (btc^{3-}: 1,3,5-benzenetricarboxylate) at 318 K (*26*), $Cr_3(btc)_2$ (*27*) at 308 K (fig. S9), and Fe-MIL-100 at 303 K (*11*). These results indicate that the propane production capacity of Fe_2(dobdc) at 318 K, which ranges up to 5.8 mol/L at a total pressure of 1.0 bar, is at least 20% higher than that of any of these other materials. A similar method was used to calculate the amount of polymer-grade (99.5%+) propylene that can be produced by these materials, again leading to a higher capacity for Fe_2(dobdc) than for any other material. The compound Mg_2(dobdc) exhibits a lower productivity than Fe_2(dobdc), a result of the lower adsorption selectivity of this material. Although zeolite ITQ-12 displayed a comparable selectivity to Fe_2(dobdc), its capacity limitation, which stems from its low pore volume of 0.134 cm^3/g, results in a propylene productivity that is just 47% of that of the metal-organic framework. For the separation of ethylene/ethane mixtures, the breakthrough simulations indicate an even greater advantage of Fe_2(dobdc) over other adsorbents, with production capacities that are roughly double those of Mg_2(dobdc) and zeolite NaX (fig. S10).

In addition to the separation of binary olefin/paraffin mixtures, there is tremendous current interest in separating ethane, ethylene, and acetylene from methane for the purification of natural gas. Indeed, a number of porous materials (*23*, *28*) are able to selectively separate methane from mixtures including C_2 hydrocarbons (ethane, ethylene, and acetylene). These materials, however, are unable to simultaneously purify the ethane, ethylene, and acetylene being removed from the gas stream. A separation process that uses the same adsorptive material for the separation and purification of all four components of a C_1/C_2 mixture could potentially lead to substantial efficiency and energy savings over current processes. To establish the feasibility of using Fe_2(dobdc) for this task, we carried out breakthrough calculations for such a mixture. Figure 4 presents simulated data on the gas-phase molar concentrations exiting an adsorber packed with Fe_2(dobdc) and subjected to a feed gas consisting of an equimolar mixture of methane, ethane, ethylene, and acetylene at a total pressure of 1 bar and a temperature of 318 K. The breakthrough times reflect the relative adsorption selectivities (acetylene > ethylene > ethane > methane) for the material, and the curves indicate a clean, sharp breakthrough transition for each successive gas.

Based on these results, the diagram at the right in Fig. 4 demonstrates how it might be possible to procure pure methane, ethane, ethylene, and acetylene using three packed beds of Fe_2(dobdc). In this process, a gas mixture is fed into the first bed, and methane—the fraction with the lowest adsorptivity—breaks through first. Pure methane can be collected until the second gas, ethane, breaks through. When the third component of the gas stream, ethylene, is present in the

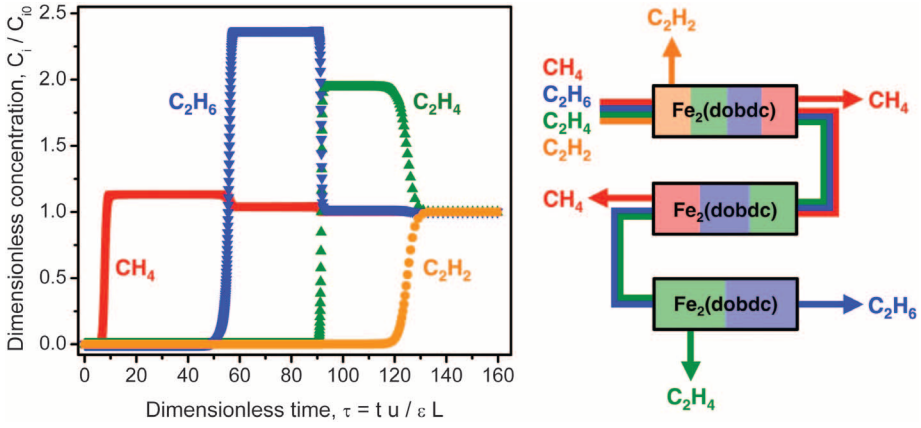

Fig. 4. (**Left**) Calculated methane (red), ethane (blue), ethylene (green), and acetylene (orange) breakthrough curves for an equimolar mixture of the gases at 1 bar flowing through a fixed bed of Fe_2(dobdc) at 318 K. (**Right**) Schematic representation of the separation of a mixture of methane, ethane, ethylene, and acetylene using just three packed beds of Fe_2(dobdc) in a vacuum swing adsorption or temperature swing adsorption process.

eluent, the gas flow is diverted to a second bed, from which additional pure methane is collected during the adsorption step and from which a mixture of ethane and ethylene is subsequently desorbed. This ethane/ethylene mixture is then separated into its pure components using a third adsorbent bed. By halting the feed into the first bed just before the breakthrough of acetylene, pure acetylene can be obtained via desorption.

Ethylene produced in a naphtha cracker contains an impurity of approximately 1% acetylene. However, there are strict limitations to the amount of acetylene that can be tolerated in the feed to an ethylene polymerization reactor. The current technology for this purpose uses absorption with liquid *N*,*N*′-dimethylformamide, but the use of solid adsorbents could potentially provide an energy-efficient alternative. We therefore also investigated the use of Fe_2(dobdc) for removal of acetylene from mixtures with ethylene. Simulated breakthrough characteristics for a feed mixture containing 1 bar of ethylene and 0.01 bar of acetylene at 318 K indicate that final acetylene concentrations on the order of 10 ppm could be realized (fig. S11).

An alternative to the use of pressure swing adsorption for olefin/paraffin separations is to adopt a membrane-based technology. To investigate the potential use of Fe_2(dobdc) membranes for the separation of such mixtures, we applied a simulation methodology previously employed for evaluating idealized Mg_2(dobdc) membranes (*29*, *30*). Here, an equimolar ethylene/ethane or propylene/propane mixture permeates through a contiguous, unsupported layer of Fe_2(dobdc) crystals, all aligned such that the channels of the framework are oriented parallel to the gas flow. Although a membrane of this type would be challenging to prepare, the following results indicate the utility of an unsupported metal-organic framework membrane. The permeation fluxes for the gas components are then related to the gradients in the loadings within the crystals by the Maxwell-Stefan diffusion equations (*29*–*31*). The calculated ethylene/ethane permeation selectivities lie in the range of 13 to 20 for total upstream pressures between 0.1 and 1.0 bar (fig. S12). These values are close to the corresponding adsorption selectivities in Fe_2(dobdc) because the more mobile partner species are slowed down within the one-dimensional channels of the structure. The slowing-down effects are caused by correlations in the molecular hops of the mobile and tardier species in the mixture within the one-dimensional channels of structures such as Fe_2(dobdc) and Mg_2(dobdc) (*31*). Such correlations serve to bring the component diffusivities in the mixture closer to each other.

In other words, strong correlation effects within the one-dimensional channels of Fe_2(dobdc) cause the permeation selectivities to be close to the adsorption selectivities, which, as discussed above, are very high. The calculated permeation selectivities are expected to be reasonably accurate, irrespective of the accuracy of the force field information, because the high degree of correlations within the channels tends to eliminate differences in the component mobilities. Thus, much greater selectivity can be expected for membranes based on Fe_2(dobdc) compared to ZIF-8, for which a permeation selectivity of 2.8 was recently reported (*32*). An important further advantage of the use of Fe_2(dobdc) is that the diffusivities within the 11 Å–wide channels of this material are about two to three orders of magnitude greater than those in ZIF-8, conferring both selectivity and permeability advantages. Similar advantages can be expected for applications of Fe_2(dobdc) in membrane separations of equimolar propylene/propane mixtures, for which permeation selectivities are calculated to lie in the range of 14 to 16 for total upstream pressures between 0.05 and 1.0 bar (fig. S13).

The foregoing results demonstrate the extraordinary prospects for using the metal-organic framework Fe_2(dobdc) as a solid adsorbent in the separation of valuable C_1 to C_3 hydrocarbons through pressure/temperature swing adsorption methods or through membrane-based applications.

References and Notes

1. R. B. Eldridge, *Ind. Eng. Chem. Res.* **32**, 2208 (1993).
2. K. Tanaka, A. Taguchi, J. Hao, H. Kita, K. Okamoto, *J. Membr. Sci.* **121**, 197 (1996).
3. D. J. Safarik, R. B. Eldridge, *Ind. Eng. Chem. Res.* **37**, 2571 (1998).
4. M. Eddaoudi *et al.*, *Science* **295**, 469 (2002).
5. S.-I. Noro, S. Kitagawa, M. Kondo, K. Seki, *Angew. Chem. Int. Ed.* **39**, 2081 (2000).
6. L. J. Murray, M. Dincă, J. R. Long, *Chem. Soc. Rev.* **38**, 1294 (2009).
7. N. L. Rosi *et al.*, *Science* **300**, 1127 (2003).
8. J.-R. Li, R. J. Kuppler, H.-C. Zhou, *Chem. Soc. Rev.* **38**, 1477 (2009).
9. Y.-S. Bae *et al.*, *Chem. Commun. (Camb.)* (35): 4135 (2008).
10. S. Bourrelly *et al.*, *J. Am. Chem. Soc.* **127**, 13519 (2005).
11. J. W. Yoon *et al.*, *Angew. Chem. Int. Ed.* **49**, 5949 (2010).
12. Z. Zhang, S. Xiang, B. Chen, *CrystEngComm* **13**, 5983 (2011).
13. S.-C. Xiang *et al.*, *Nat. Commun.* **2**, 204 (2011).
14. H. Leclerc *et al.*, *Phys. Chem. Chem. Phys.* **13**, 11748 (2011).
15. R. Matsuda *et al.*, *Nature* **436**, 238 (2005).
16. E. D. Bloch *et al.*, *J. Am. Chem. Soc.* **133**, 14814 (2011).
17. Z. Bao *et al.*, *Langmuir* **27**, 13554 (2011).
18. Y.-S. Bae *et al.*, *Angew. Chem. Int. Ed.* **51**, 1857 (2012).
19. A. Fürstner *et al.*, *J. Am. Chem. Soc.* **130**, 8773 (2008).
20. H. Wu, W. Zhou, T. Yildirim, *J. Am. Chem. Soc.* **131**, 4995 (2009).
21. R. Krishna, J. R. Long, *J. Phys. Chem. C* **115**, 12941 (2011).
22. A. L. Myers, J. M. Prausnitz, *AIChE J.* **11**, 121 (1965).
23. S. H. Hyun, R. P. Danner, *J. Chem. Eng. Data* **27**, 196 (1982).
24. J. J. Gutiérrez-Sevillano *et al.*, *J. Phys. Chem. C* **114**, 14907 (2010).
25. M. C. Das *et al.*, *Chemistry* **17**, 7817 (2011).
26. M. G. Plaza *et al.*, *Micropor. Mesopor. Mater.*, published online 14 July 2011.
27. L. J. Murray *et al.*, *J. Am. Chem. Soc.* **132**, 7856 (2010).
28. S. C. Reyes *et al.*, U.S. Patent 12,322,364 (2009).
29. R. Krishna, J. M. van Baten, *J. Membr. Sci.* **377**, 249 (2011).
30. R. Krishna, *J. Phys. Chem. C* **113**, 19756 (2009).
31. R. Krishna, J. M. van Baten, *J. Membr. Sci.* **383**, 289 (2011).
32. H. Bux, C. Chmelik, R. Krishna, J. Caro, *J. Membr. Sci.* **369**, 284 (2011).

Acknowledgments: The data described in this paper are presented in the supporting online material. This research was supported through the Center for Gas Separations Relevant to Clean Energy Technologies, an Energy Frontier Research Center funded by the U.S. Department of Energy, Office of Science, Office of Basic Energy Sciences under award DE-SC0001015. In addition, we thank the National Institute of Standards and Technology National Research Council Postdoctoral Fellowship Research Associate program for support of W.L.Q.; V. K. Peterson and S. N. Maximoff for assistance and helpful discussions; C. J. Kepert for the use of his glovebox to prepare neutron powder diffraction samples; and J. M. van Baten for valuable assistance in the simulation work. Metrical data for the solid-state structures of the acetylene, ethylene, ethane, propylene, and propane adducts of Fe_2(dobdc) are available free of charge from the Cambridge Crystallographic Data Centre under reference numbers CCDC 866357 to 866361. The authors and the University of California, Berkeley have filed a patent on the results presented herein.

Supporting Online Material

www.sciencemag.org/cgi/content/full/335/6076/1606/DC1
Materials and Methods
Figures S1 to S13
Tables S1 to S23
Movies S1 to S11
References (*33*–*45*)

6 December 2011; accepted 16 February 2012
10.1126/science.1217544

$^{238}U/^{235}U$ Systematics in Terrestrial Uranium-Bearing Minerals

Joe Hiess,[1]* Daniel J. Condon,[1] Noah McLean,[2] Stephen R. Noble[1]

The present-day $^{238}U/^{235}U$ ratio has fundamental implications for uranium-lead geochronology and cosmochronology. A value of 137.88 has previously been considered invariant and has been used without uncertainty to calculate terrestrial mineral ages. We report high-precision $^{238}U/^{235}U$ measurements for a suite of uranium-bearing minerals from 58 samples representing a diverse range of lithologies. This data set exhibits a range in $^{238}U/^{235}U$ values of >5 per mil, with no clear relation to any petrogenetic, secular, or regional trends. Variation between comagmatic minerals suggests that $^{238}U/^{235}U$ fractionation processes operate at magmatic temperatures. A mean $^{238}U/^{235}U$ value of 137.818 ± 0.045 (2σ) in zircon samples reflects the average uranium isotopic composition and variability of terrestrial zircon. This distribution is broadly representative of the average crustal and "bulk Earth" $^{238}U/^{235}U$ composition.

The uranium-lead (U-Pb) system is widely used as an isotopic chronometer for geological and meteoritic materials that are less than 1 million to greater than 4.5 billion years old. This system is particularly useful because it has two long-lived isotopes, ^{238}U and ^{235}U,